Computational Materials Science 258 (2025) 114046

Contents lists available at ScienceDirect

Computational Materials Science

journal homepage: www.elsevier.com/locate/commatsci

Full length article

Molecular level dependencies of water permeability in di-block copolymer assemblies

Kourosh Hasheminejad [a,b], Ygor Morais Jaques [a,b], Anneli Lepo [c], Alberto Scacchi [a,b,d], Maria Sammalkorpi [a,b,*]

[a] Department of Chemistry and Materials Science, Aalto University, P.O. Box 16100, FI-00076 Aalto, Finland
[b] Academy of Finland Center of Excellence in Life-Inspired Hybrid Materials (LIBER), Aalto University, P.O. Box 16100, FI-00076 Aalto, Finland
[c] R&D and Technology, Kemira Oyj, P.O. Box 44, FI-02271 Espoo, Finland
[d] Department of Mechanical and Materials Engineering, University of Turku, Vesilinnantie 5, FI-20014 Turku, Finland

ARTICLE INFO

Keywords:
Hydrophobic coatings
Di-block copolymers
Moisture barrier
Molecular dynamics simulations

ABSTRACT

Atomistic detail molecular dynamics (MD) simulations were used to examine molecular level dependencies of water interactions and permeability of amphiphilic di-block copolymer assemblies. Four different linear amphiphilic di-block copolymers, with chemically identical hydrophilic blocks but varying hydrophobic blocks, were studied. The simulations show that while all examined di-block copolymers formed assemblies highly efficient in blocking water, the ability of the assemblies to sustain their water blocking character when subject to lateral strain had significant differences. The assemblies retaining high internal order under lateral strain were most efficient in moisture blocking. In this, flexible side chains with branching filling the surroundings with hydrophobic groups to prevent molecular level water penetration, were important. Moreover, styrene rings provided efficient, space-filling moisture protection blocks, demonstrating further the importance of flexible spatial orientation hydrophobic side chains. The simulations also connect the roughness and interfacial fluctuations of the block-copolymer assembly with water penetration. The work shows molecular level design principles for enhancing moisture preventing coatings and gives insight into engineering the performance of other filtration systems.

1. Introduction

Polymeric assemblies and membranes provide selective barriers and protective coatings for a variety of applications, ranging from water purification to food packaging [1–6]. Often, selective blocking or passage of substances through the polymer material is targeted. Particularly interesting for enhanced selectivity are block copolymer membranes, since they provide highly controllable self-assembly structure [7,8]. For example, block copolymer systems allow targeting uniform pore size and tunable surface porosity [5,8–12], but also control over domain formation and segregation in the assembly [13–16]. However, optimizing the systems in terms of permeability and selectivity, long-term stability, economic considerations, and sustainability remains a challenge. For a recent review on polymer membranes, see Ref. [7].

Here, we employ molecular modelling to gain insight into block copolymer assemblies, especially from the point of view of moisture blocking applications, i.e. water penetration. Polymeric coatings with moisture blocking properties are particularly important in food packaging and paper industries, but also in preventing corrosion [17–20]. At a basic level, insight into water mobility in a polymer assembly can be obtained by classic diffusion considerations, such as Fick's law. Essential factors to the permeability are solubility and diffusivity of the substance of interest in the polymeric assembly [17]. This means that the water blocking performance of block copolymer coatings depends on the chemical nature of both polymeric components and the fluid of interest, the degree of crystallinity of the polymer material, the affinity of the polymeric components to the fluid (in the case of water, polarity), but also the molecular weight and the polydispersity of the polymer [7,17,21–23]. Enhanced barrier properties can be achieved by structure manipulation, such as manufacturing multi-phase and multi-layer films through controlled assembling and blending. For example, an aligned polymer matrix provides improved water blocking performance due to an increase in crystallinity, reduced free volume, and hindered diffusion within the polymeric films. For reviews on the topic, see Refs. [7,17,24].

Wetting of polymeric films also depends on, e.g. the contact angles formed between a water droplet and the film surface, the spreading of

* Corresponding author at: .
E-mail address: maria.sammalkorpi@aalto.fi (M. Sammalkorpi).

https://doi.org/10.1016/j.commatsci.2025.114046
Received 28 April 2025; Received in revised form 10 June 2025; Accepted 10 June 2025
Available online 27 June 2025

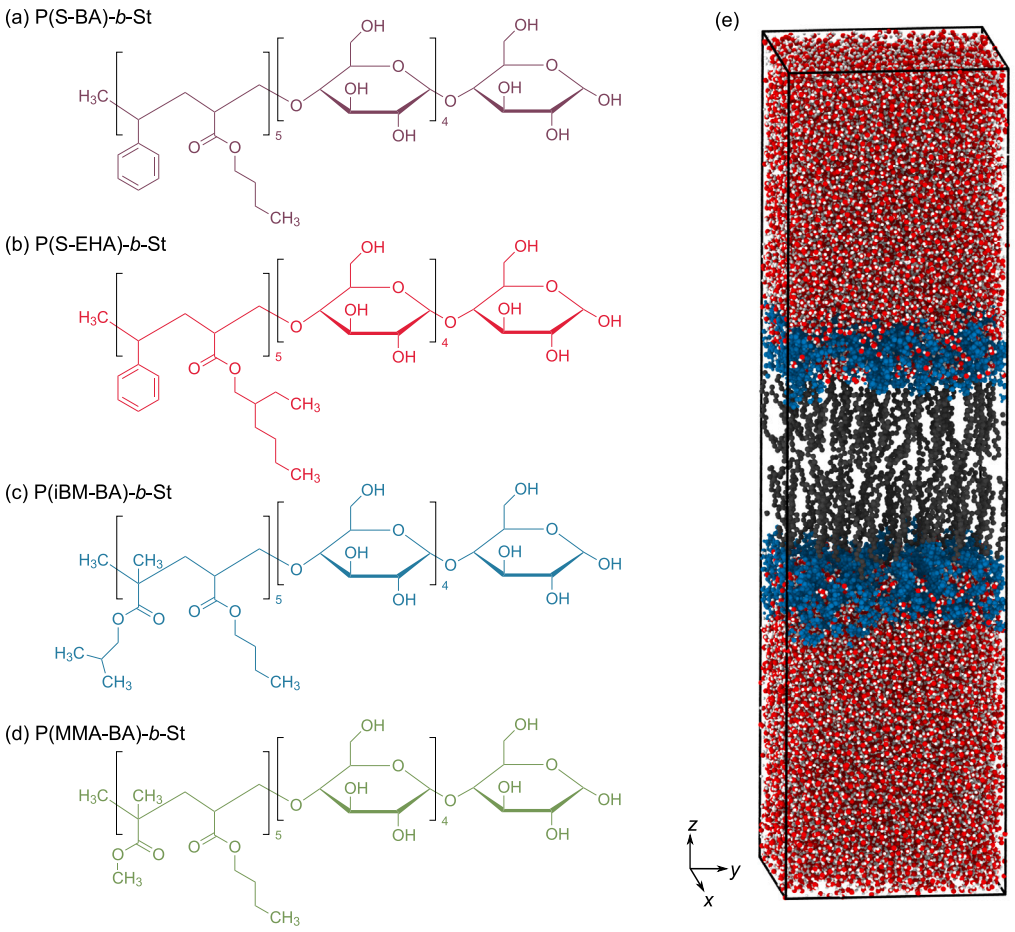

Fig. 1. Chemical structures of the examined amphiphilic di-block copolymers and a visualization of a representative system. The molecular structures are alternating (a) poly(styrene-*co*-n-butyl acrylate)-*b*-starch, (b) poly(styrene-*co*-2-ethylhexyl acrylate)-*b*-starch, (c) poly(iso-butyl methacrylate-*co*-n-butyl acrylate)-*b*-starch, and (d) poly(methyl methacrylate-*co*-n-butyl acrylate)-*b*-starch. Each di-block copolymer contains in total 5 repeat units of the hydrophobic two-monomer alternating block, 10 monomers in total, and 5 starch hydrophilic monomers. (e) Visualization of a representative simulation system. The explicit water molecules (red and white), the hydrophilic blocks (blue), and the backbones of the hydrophobic blocks (dark gray) are shown. The hydrophobic blocks side groups are omitted in the visualization for clarity.

the droplet over the film surface, and surface roughness at micro/nano scale [25–29]. Experimentally, the diffusion of water into polymeric assemblies is examined via, e.g., pulsed field gradient nuclear magnetic resonance spectroscopy [30], attenuated total reflectance Fourier transform infrared spectroscopy [31–33], polarized Raman spectroscopy [34], neutron reflectometry [35], and neutron scattering [36] approaches. As water penetration into polymeric assemblies depends on the surface topology and structural characteristics of the surface, scanning electron microscopy, atomic force microscopy, and transmission electron microscopy are employed along with X-ray and neutron scattering techniques [37–39].

It is evident that the chemistry of the polymers strongly affects water interactions by miscibility considerations and steric barriers. For example, both methyl groups and bulky polar side groups can provide low water permeability [21,40,41]. At the microstructural level, inefficient polymer chain packing, i.e. local density differences, enhances water diffusivity [42]. More macroscopically, pores and structural defects in the polymeric assemblies targeting moisture protection enhance water penetration [43]. Besides the assembly structure, its dynamics also influence the molecular-level mobility of water molecules: for example, the transition from glassy to rubbery chain dynamics promotes chain movements, and consequently water diffusion, as the chains can carry water molecules [21,44,45].

Polymeric materials, including polymeric membranes and other assemblies, pose a challenging multi-scale soft materials modelling problem since their spatiotemporal response typically depends on multiple co-existing length and time scales (see, e.g. Refs. [7,46,47]). Theoretical models and computer simulations relying on them are limited to describing phenomena in the operational range of the model in terms of length and time scale. Despite this, computer simulations and theoretical approaches have proved to be useful for predicting assembly structures and morphologies [48,49], including porosity and domain formation characteristics [50–53], but also microstructural dependencies [54,55]. In terms of permeability, advanced diffusion considerations in polymeric media exist [36,56–62]. Such approaches provide general predictions of the macroscopic permeability response based on statistical and macroscale averaged materials properties. However, at the microscopic level, moisture blocking properties arise from molecular level dependencies and microstructural mechanisms. Molecular level modelling, with explicit temporal dynamics, in practice molecular dynamics, has been used to extract such information [63–67]. Atomistic detail molecular modelling has been used to examine small molecule transport in both lipid membranes [68–72] and in polymer assemblies [73–78]. Water binding and mobility have also been modelled in the context of hydrated polyelectrolyte assemblies, connecting the thermal plasticization response to water mobility and water at intrinsic ion pairs [55,79], but also demonstrating the differences in water mobility and local diffusion arising from polymer chemistry [54,55].

For developing moisture protecting coatings, amphiphilic di-block copolymers are particularly interesting since they provide simple, well-controlled model systems, that can self-assemble on surfaces to form uniform hydrophobic layers [50,51,80,81]. They have also attained simulations attention. For example, combining MD simulations and small-angle neutron scattering has shown that water molecules in

block copolymer assemblies are likely confined to the hydrophilic layer. Their dynamics change at the hydrophobic/hydrophilic interface [77]. Also, the block copolymer architecture affects water interactions, mainly via packing and steric interactions. For example, the long hydrophilic chains act as a physical barrier (water molecule motion is hindered) [82]. The packing and steric interactions also explain why symmetric amphiphilic di-block copolymers form uniform lamellar membranes or films with good blocking properties via self-assembly, as shown by coarse-grained simulations [50,51,83].

However, molecular level dependencies on moisture prevention, as well as the factors governing the efficiency of moisture blocking response, remain open questions. To address this, we examine here four chemically distinct di-block copolymer coatings. The coatings are compared for their water interactions, especially water penetration, together with the molecular origins of their performance. The performed MD simulations provide a highly detailed, microscopic view that reveals the mechanisms and dependencies of the observed response, providing guidelines for optimizing the practical usability of such coatings.

2. Simulation system and computational methods

The studied copolymer components are selected since they are commonly used in producing protective coatings in paper industries [84,85]: the studied copolymers are summarized in Fig. 1. We have selected starch (St) as the hydrophilic block for all systems, as it is a readily available, cheap natural polysaccharide commonly used in coating processes [86]. The hydrophobic block is itself a copolymer, and we examined four variations. The examined variations are alternating (1) styrene (S) and n-butyl acrylate (BA) [87], (2) styrene and 2-ethylhexyl acrylate (EHA) monomers [88,89], (3) iso-butyl methacrylate (iBM) and n-butyl acrylate, and (4) methyl methacrylate (MMA) and n-butyl acrylate [90–93]. That is, (1) and (2) both have S monomers yet combined with monomers with side chains of different lengths (BA and EHA), while (3) and (4) both have BA monomers yet combined with iBM and MMA, respectively. This choice enables a systematic comparison of both steric packing and hydrophobicity differences, but also the resilience to non-ideal packing. The choice to systematically use an alternating copolymer structure is a modelling approximation intended to describe an even distribution of the monomers while best reflecting in the short oligomeric chain the typically random copolymer structure these components have in synthesized copolymers.

All-atom, explicit solvent MD simulations of amphiphilic di-block copolymer assemblies in water were performed using LAMMPS [94] with the OPLS-AA force field [95–97] and TIP3P [98] water model. Bilayer-like assemblies made of four different copolymers with approximately the same length were examined. The copolymers were constructed by covalently bonding similar absolute length hydrophobic and hydrophilic blocks to each other: 10 monomers for the hydrophobic block and 5 monomers for the hydrophilic block (starch) as the monomer sizes differ. This is motivated by symmetric (in length) amphiphilic di-block copolymers promoting the formation of uniform layers, which potentially improves blocking properties in previous works [50,51,80,99]. Table 1 provides a summary of the examined copolymers, their abbreviated names, and the size of the equilibrated simulation boxes. The selected box sizes are sufficient to capture local packing of the short chain segments. This enables to model the key water penetration and structural reorganization response changes between the systems. However, the simplified, microscopic modelling setup fails to capture macroscopic system size and chain length driven variety of conformations in the polymers and larger scale fluctuations.

The bilayer-like assemblies were constructed from two leaflets of initially axially straight, parallel, and energy-minimized copolymers. Each leaflet comprises of 49 chains with their hydrophobic segments sandwiched between the hydrophilic layers. To form the leaflets, the copolymer chains were placed in a regular honeycomb lattice inside a rectangular simulation box ≈10% larger than the equilibrated system laterally (x and y dimensions). The chains were rotated axially by a random angle value to randomize the side chain orientations. Finally, 10 000 water molecules were randomly placed on each side of the assembly, ensuring that none were positioned inside the hydrophobic layer. This was done under the constraint that each water molecule must maintain a minimum distance of 2 nm from the hydrophobic layer.

The copolymers and the simulation setups were constructed by combining Avogadro [100], Moltemplate [101], and Packmol [102]. Ovito [103] was used for visualization, while MDAnalysis python package [104,105] was used for part of the analysis.

Periodic boundary conditions were employed in all directions. All simulations were carried out at a temperature of 298 K and at a pressure of 1 atm. Nosé-Hoover thermostat [106,107] and barostat [108] were used, with the temperature damping parameter of $100\times dt$ and pressure damping parameter of $1000 \times dt$, where dt is the time-step. Van der Waals and Coulombic interactions were calculated up to a cut-off of 1 nm in real space, whereas for the long-range Coulombic contributions, the particle–particle particle-mesh (pppm) algorithm was used, with accuracy of 10^{-4}. A conjugate gradient algorithm was used for energy minimization.

The initial relaxation/equilibration of the systems was performed by repeating 6 times on each single system a procedure in which an energy minimization step was followed by a 0.5 ns isothermal–isobaric (NpT) simulation. After this, each simulation was continued for 1 ns in the NVT ensemble, followed by 1 ns in the NpT ensemble. The multistep initial system preparations protocol with the 6 repeat cycles was executed to compactify the initially approximately 10% larger than equilibrium size simulation box to a density that no longer showed structural evolution. All systems were relaxed employing the same procedure. We checked all systems before the start of the production runs to ensure that no water molecules were inside the hydrophobic layer after the initial relaxation protocol. A representative snapshot of the system after relaxation is shown in Fig. 1(e).

After the equilibration, the simulation system sizes vary slightly dependent on the polymer species. The values reported in Table 1 correspond to the simulation box dimensions after the final 1 ns NpT simulation in the initial equilibration protocol. In all cases, initial preparation steps used an integration time-step of 1 fs. The production runs were carried out for 100 ns in the NpT ensemble with a time-step of 2 fs. The first 60 ns of the trajectories is omitted, and the last 40 ns of production runs were used for all analyses.

To study the response of the assemblies under mechanical strain and non-ideal packing structures, the relaxed simulation boxes were stretched by 2, 6, and 10% bi-axially in the x and y directions. These non-ideal conditions can be connected with realistic situations in applications, where, e.g. due to mechanical stress, such as folding and creasing, the polymer assembly is stretched from its original structure. The stretching was performed dynamically with a constant rate over a time period of 500 ps. During this, no water molecules penetrated the hydrophobic layer. Notably, the stretching speed is such that the chain segments of the systems do not have time to relax, except for small local movements: the outcome is similar to scaling of coordinates for instantaneous stretching. After the dynamic stretching was completed to the desired system size, the size of the boxes was kept fixed along the xy-plane but allowing z-axial pressure equilibration via anisotropic pressure control in the NpT ensemble. The systems were relaxed for 1 ns. This time is sufficient to equilibrate the water density in the systems, assessed by z-axis density changes.

Density profiles along the z-axis were obtained by binning the simulation system in the xy-plane into slices of 0.2 Å. The 2D density (xy-plane) data employed a 0.5 × 0.5 Å^2 square bin. The roughness factor of the hydrophobic/hydrophilic interface is measured as the ratio of the actual area of the hydrophobic layer surface facing the hydrophilic segments and the area of the xy-plane of the simulation

Table 1
Summary of the amphiphilic di-block copolymers, including their abbreviated name, the length of each segment, and the corresponding size of the equilibrated simulation box. In all cases, 10 hydrophobic monomers are covalently bonded to a starch block of 5 monomers, resulting in copolymers that are approximately symmetric in their hydrophobic to hydrophilic segment lengths. The presented box size corresponds to the system size at the end of the relaxation protocol (beginning of production run).

Amphiphilic di-block copolymer	Abbreviation	Hydrophobic length (monomers)	Hydrophilic length (monomers)	Relaxed simulation box size $(nm)^3$
Poly(styrene-*co*-n-butyl acrylate)-*b*-starch	P(S-BA)-*b*-St	10	5	$6.08 \times 6.16 \times 23.50$
Poly(styrene-*co*-2-ethylhexyl acrylate)-*b*-starch	P(S-EHA)-*b*-St	10	5	$6.61 \times 6.61 \times 21.33$
Poly(iso-butyl methacrylate-*co*-n-butyl acrylate)-*b*-starch	P(iBM-BA)-*b*-St	10	5	$6.49 \times 6.14 \times 22.84$
Poly(methyl methacrylate-*co*-n-butyl acrylate)-*b*-starch	P(MMA-BA)-*b*-St	10	5	$6.08 \times 6.07 \times 23.50$

box [109], and was calculated using the alpha-shape algorithm of the *construct surface mesh tool* in Ovito [103], see Ref. [110]. A probe sphere with a radius of 3.5 Å was used [111].

The radius of gyration of chain j was calculated as

$$R_j^{\mathrm{g}} = \sqrt{\frac{\sum_{i=1}^{N_j} m_i \left(\mathbf{r}_i - \mathbf{r}_j^{\mathrm{cm}}\right)^2}{\sum_{i=1}^{N_j} m_i}}, \tag{1}$$

where m_i is the mass of atom i belonging to chain j, and $\mathbf{r}_i$ its position, while $\mathbf{r}_j^{\mathrm{cm}}$ is the centre of mass for the chain j and N_j its number of atoms.

The mean square displacement (MSD) was calculated as

$$\mathrm{MSD}(t) = \frac{1}{N_p} \sum_{i=1}^{N_p} \left[\frac{1}{N_t} \sum_{t_0} |\mathbf{r}_i(t+t_0) - \mathbf{r}_i(t_0)|^2 \right], \tag{2}$$

where N_p is the number of particles, N_t is the number of initial time origins t_0 (reference time from which particle displacements are measured) used for the inner summation, and $\mathbf{r}_i(t+t_0)$ and $\mathbf{r}_i(t_0)$ are the positions of particle i at times $t+t_0$ and t_0, respectively. Note that the term inside the brackets, including the inner sum, represents the time average over different lag-times with length t (done to increase the data statistics), while the outer sum represents the ensemble average over particles [112]. As the number of initial time origins t_0 becomes small when t is increased, the MSD values are expected to fluctuate more as t approaches the total length of the production run time. The MSD data has been fitted using the following empirical single exponential equation, see e.g. Ref. [113],

$$\mathrm{MSD}(t) = A\left(1 - e^{-kt}\right) + C. \tag{3}$$

In this, A is the amplitude, C is the baseline offset, and k is the growth constant. This form is used as a best fit to data, but it does not have a physical consideration basis.

Molecular level water movement in the system was examined by evaluating the survival probability of water molecules in a specific region. This probability is defined as the ratio of particles that remain in the region of interest after a time interval τ, $n_{\tau_0}(\tau_0+\tau)$, and the number of particles initially present at time τ_0, $n_{\tau_0}(\tau_0)$. This ratio is averaged over different initial times τ_0, resulting in the survival probability

$$P(\tau) = \frac{1}{N_{\tau_0}} \sum_{\tau_0=0}^{N_{\tau_0}} \frac{n_{\tau_0}(\tau_0+\tau)}{n_{\tau_0}(\tau_0)}. \tag{4}$$

Here N_{τ_0} is the number of initial times considered. A slow decay of $P(\tau)$ indicates that the retention times of water molecules in the region are long, whereas a fast decay corresponds to shorter retention times [114].

All z-axial density characterizations are mirrored such that only the data for the positive axis (half of the simulation system) is presented. The plane $z = 0$ is set to reside in the center of the simulation box, i.e. in the middle between the two hydrophobic leaflets of the di-block copolymer assembly.

The end-to-end distance for each respective block is calculated as the average distance between the first and last backbone carbon atom of the block segment. The position of the hydrophobic/hydrophilic interface is calculated as the average z-axial position of the linker carbon atoms connecting the hydrophobic and hydrophilic segments in the copolymer chains. A water molecule is considered to be located in the hydrophobic layer if its oxygen atom z-coordinate is between the two hydrophobic/hydrophilic interfaces.

3. Results

3.1. Polymer assemblies structure and water interactions

The z-axial density distribution profiles of the examined di-block copolymer systems are presented in Fig. 2. In all cases, the di-block copolymer systems are relatively uniform, qualitatively similar, stable lamellar structures that are surrounded by bulk water. The data shows that the hydrophobic segments of the di-block copolymer chains are well-packed, and segregated from the starch slab, and this region remains devoid of water molecules. However, the data also shows that water readily penetrates the hydrophobic/hydrophilic interface. Throughout the 100 ns simulation time, these stable bilayer-like assembly structures persist.

The density of the studied hydrophobic layers is $\approx$1.1 $\mathrm{g/cm^3}$ in all cases. The hydrophobic segments of the di-block copolymers are more bulky in terms of xy-plane packing than the starch segments in the layered structure, controlling the simulation box size in the xy-plane, and thus setting the lateral space available for the hydrophilic segments. Table 1 collects the differences in simulation system sizes. Consequently, the starch layer structure is strongly affected by the chemistry of the hydrophobic segments, as the two blocks are tethered together. This is also evident in the amount of water penetrating the starch layer to the hydrophobic/hydrophilic interface, Fig. 2.

Although no significant water penetration to the hydrophobic layer takes place during the simulations, see Fig. 2, the examined systems differ in water molecules in the hydrophobic layers. Fig. 3 shows the number of water molecules in the hydrophobic layers normalized by the area of the xy-plane, A_{xy}, of the corresponding setup. The P(S-EHA)-*b*-St and P(iBM-BA)-*b*-St copolymers allow the least penetration of water molecules into the hydrophobic region of the assembly. On the other hand, penetration is more pronounced for the P(S-BA)-*b*-St and P(MMA-BA)-*b*-St copolymers. The findings can be understood considering the size of the side groups of the different hydrophobic blocks, and the overall physical and chemical properties of the chains: steric hindrance, combined with the hydrophobicity characteristics related to observed water penetration in simulations here.

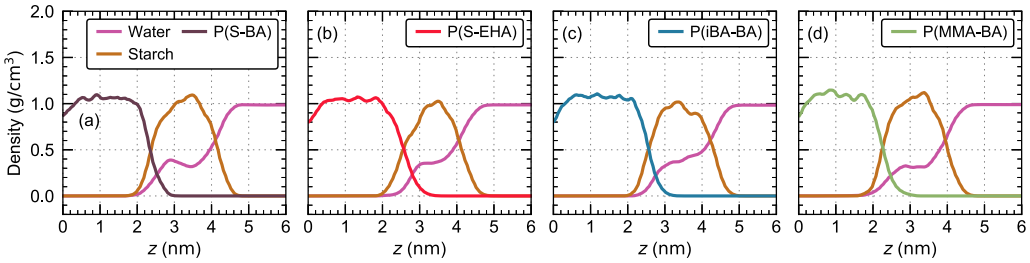

Fig. 2. The z-axial density profiles in the MD simulations calculated for (a) P(S-BA)-*b*-St, (b) P(S-EHA)-*b*-St, (c) P(iBM-BA)-*b*-St, and (d) P(MMA-BA)-*b*-St assemblies. The systems correspond to 0% lateral strain (no stretching).

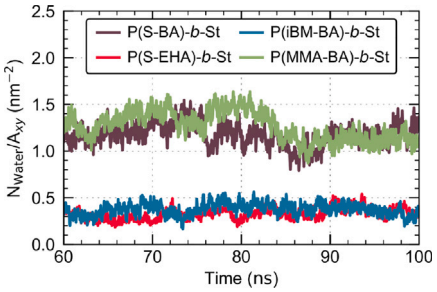

Fig. 3. Water blocking performance of the modelled systems. The number of water molecules in the hydrophobic layers during the last 40 ns of the simulations normalized by the area of the xy-plane of each simulation box. The systems correspond to 0% lateral strain (no stretching).

3.2. Effects of stretching on the assemblies

3.2.1. Structural changes

To assess at a simplified level the effect of imperfections and non-idealities in polymer film structures, the assemblies are next stretched 2, 6, and 10% along the x- and y-axial directions, with both axes stretched the same amount (xy-plane stretching). This allows an assessment of the water interactions changes and blocking characteristics persistence under non-ideal chain packing.

Fig. 4 shows the z-axial density profiles of the P(S-BA)-*b*-St assembly under different xy-plane bi-axial stretching conditions. Corresponding data for the other studied compositions is provided in Figure S1 of the Supporting Information (SI). The data shows that stretching results in a decrease in the hydrophobic layer thickness, as expected, yet its density remains relatively constant. This suggests that the layer structure relaxes efficiently, but is also a direct indication that the conformations and orientations of the hydrophobic segments change. At the practical level, this means that the hydrophobic layer can be stretched without cracking the hydrophobic layer. Note that we examined deformations up to 10%, however, the 100 ns simulation time duration is so short that instabilities leading to membrane rupture will not show during the simulation time, especially in a periodic simulation system where the periodic boundary conditions suppress structural fluctuations.

For all systems, the starch layer also responds to stretching: as expected, the polymer chain packing density of the hydrophilic layer decreases when stretched, but also the starch chains tend to lean towards the interface due to the extra space generated. Figure S2 of the SI presents 2D density maps of the hydrophilic layer calculated along the xy-plane for all the examined systems: when unstretched, the starch layers in the membranes are more packed, and consequently, there are fewer paths for water to reach the interface. On the other hand, at 10% stretching, starch packs more heterogeneously, providing more ways for water to pass through the membrane. With this, also the density of starch is decreased, which contributes to an enhanced water penetration towards the interface.

3.2.2. Conformations of the hydrophobic backbones

Stretching of the assemblies also affects the conformations of the hydrophobic blocks. Fig. 5 shows this by the backbone orientation angle distributions and the spatial localization of the hydrophobic block backbones for unstretched and 10% stretched systems. The backbone orientation angle θ is calculated as the angle between the z-axis and the vector defined by the positions of the first and last backbone carbon atom in each hydrophobic segment. While the backbone angle distribution of P(S-EHA)-*b*-St assembly is relatively insensitive to stretching, the P(S-BA)-*b*-St, P(iBM-BA)-*b*-St, and P(MMA-BA)-*b*-St copolymers show significant tilting of their hydrophobic chains when the assembly is stretched. The effect of the change is quantified by MSD of the hydrophobic backbones, see Figure S3 of the SI. Following the angle distribution, the P(iBM-BA)-*b*-St assembly is most affected by stretching. The styrene monomers and bulky side groups in the hydrophobic segment of P(S-EHA)-*b*-St assembly help stabilize the structure due to physical interlocking of the chains. However, the P(iBM-BA)-*b*-St shows an opposite response, with low rigidity resulting in the most noticeable packing disorder when stretched.

The 2D density maps of Fig. 5 show the stability and structural rigidity differences in the hydrophobic backbone packing for the 0% and 10% stretchings. While sharp-edged high-density regions in the colour maps indicate that the hydrophobic chains hold their position and orientation during the 40 ns analysed time period, smoothening of the density map indicates a local movement of the chains. For all systems, stretching increases the delocalization of the hydrophobic material, indicating that the hydrophobic chains move more. Outlier in this, P(S-EHA)-*b*-St persists in its structural features despite the stretching. Overall, the findings are consistent with the observed decrease in end-to-end distance and radius of gyration with stretching (Table 2). Direct interpretation is that the hydrophobic backbones bend to cover the extra volume created by the stretching. Altogether, Fig. 5 shows that the side chains in the hydrophobic blocks determine the response of the membranes to external forces.

3.2.3. Morphology of the hydrophobic/hydrophilic interface

The morphology of the hydrophobic/hydrophilic interface affects the water penetration into the hydrophobic layer. To characterize this interface, we calculated the roughness factor for both unstretched and 10% stretched systems and the corresponding water penetration data for the 10% stretched system, see Fig. 6 and Figure S4 of the SI. The data shows that for the P(S-BA)-*b*-St and P(S-EHA)-*b*-St systems, the roughness decreases with stretching. Conversely, P(iBM-BA)-*b*-St and P(MMA-BA)-*b*-St show increasing interfacial roughness due to stretching. It is sensible to assume that high roughness implies easier water penetration through the interface [26]. Consistent with this, indeed, the number of water molecules in the hydrophobic layers, Figure S4 of the SI, and the corresponding radial distribution function $g(r)$ calculated between the hydrophobic backbones and water molecules, Fig. 6(c), show that the P(S-EHA)-*b*-St has the lowest number of water molecules in contact with the hydrophobic layer. Additionally, P(S-EHA)-*b*-St also shows the largest estimated effective interfacial tension at the water-hydrophobic layer interface of the examined block copolymer systems,

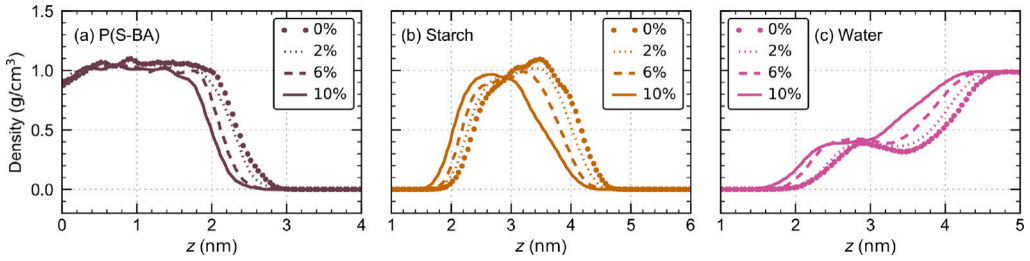

Fig. 4. The effect of xy-plane bi-axial stretching on the z-axial density profiles of the P(S-BA)-*b*-St assemblies. Panel (a) shows the hydrophobic P(S-BA), (b) the hydrophilic starch, and (c) the water density profiles in the simulation systems at 0, 2, 6, and 10% stretching of the simulation box along the x- and y-axis each.

Table 2
Effect of stretching from 0% to 10% on the hydrophobic block conformations and water penetration to the hydrophobic layers of the different polymer assemblies. Data shows end-to-end distance and radius of gyration of the hydrophobic polymer blocks. The corresponding water molecule count normalized by the surface area of the simulation boxes (xy-plane) is also reported.

Polymer system	Stretching	End-to-end distance (nm)	Radius of gyration (nm)	Water count (nm^{-2})
P(S-BA)-*b*-St	0%	2.18 ± 0.13	0.80 ± 0.02	1.18 ± 0.14
	10%	2.02 ± 0.24	0.76 ± 0.03	1.93 ± 0.22
P(S-EHA)-*b*-St	0%	2.12 ± 0.13	0.86 ± 0.03	0.33 ± 0.07
	10%	1.98 ± 0.24	0.80 ± 0.04	0.92 ± 0.13
P(iBM-BA)-*b*-St	0%	2.29 ± 0.11	0.84 ± 0.02	0.38 ± 0.08
	10%	2.14 ± 0.17	0.79 ± 0.04	2.00 ± 0.20
P(MMA-BA)-*b*-St	0%	2.08 ± 0.22	0.80 ± 0.04	1.27 ± 0.17
	10%	1.89 ± 0.31	0.75 ± 0.05	1.92 ± 0.24

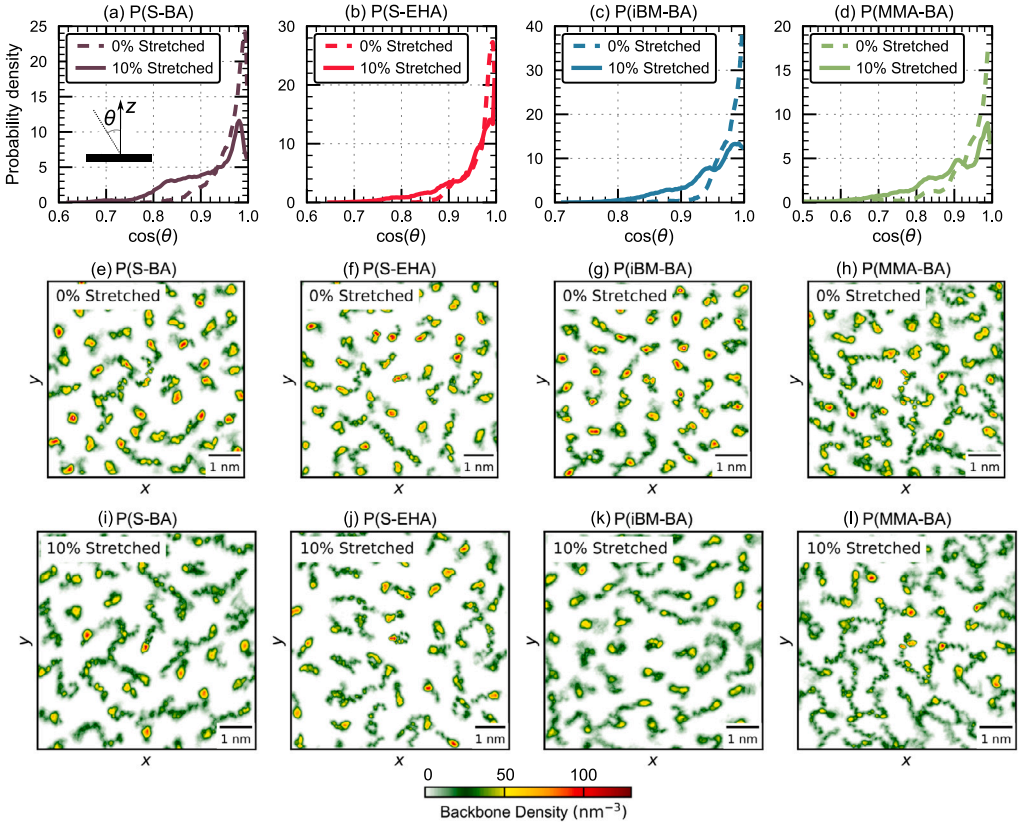

Fig. 5. Effect of stretching on tilting and spatial localization of the hydrophobic block backbones. Panels (a)–(d) present the distributions of $\cos(\theta)$, where θ is the angle between the hydrophobic backbone and the z-axis for (a) P(S-BA)-*b*-St, (b) P(S-EHA)-*b*-St, (c) P(iBM-BA)-*b*-St, and (d) P(MMA-BA)-*b*-St assemblies. Panels (e)–(l) present the spatial localization of the hydrophobic block backbones as 2D density maps for the 0% and 10% stretched systems.

see Figure S5 of the SI. Opposite to this, significantly higher water penetration can be observed for P(S-BA)-*b*-St, P(iBM-BA)-*b*-St, and P(MMA-BA)-*b*-St. For a comparison of the structural rigidity changes, see Table 2. Notably, the $g(r)$ data shows that stretching changes the order of backbone wetting, as evident in Fig. 6(c).

Altogether, the data shows that styrene makes the assemblies more resilient to uneven packing and stretching. The styrene rings form a very stably packed hydrophilic-hydrophobic segment interface that efficiently blocks water. This interface is also persistent in stretching and deformations due to the flexibility of the side chain.

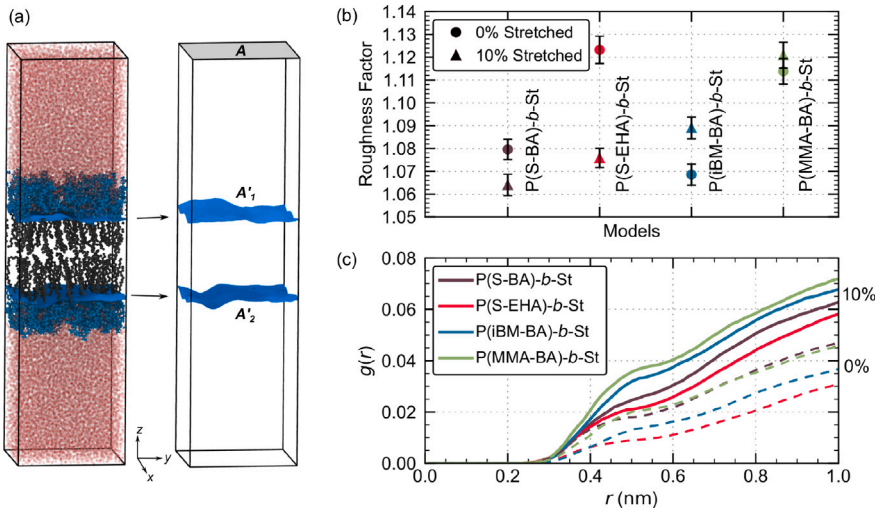

Fig. 6. (a) Schematic of the calculation of the roughness factor. The projected hydrophobic-hydrophilic interfacial surface on the hydrophobic layer is shown as blue surface planes in a sample simulation system. The roughness factor is calculated as $(A'_1 + A'_2)/2A$, where A is the xy-plane area of the simulation box and A'_1 and A'_2 are the actual areas of the hydrophobic-hydrophilic interfacial surfaces at each leaflet of the polymer assembly. (b) The roughness factors corresponding to the 0% and 10% stretched systems. (c) Water contacts determined for the 0% (dashed lines) and 10% (solid lines) stretched states for each system presented by the radial distribution function $g(r)$ calculated between the water molecules and the carbon atoms of the hydrophobic block backbones.

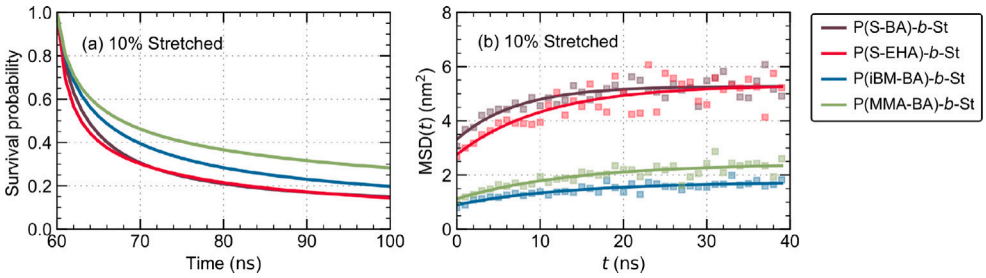

Fig. 7. (a) Water molecule survival probability vs. time and (b) water molecule MSD. Both data sets are calculated for water molecules in the hydrophobic layers in the 10% stretched systems. The MSD data fits follow Eq. (3). The fitting parameter values are provided in the SI.

3.2.4. Water interactions in the hydrophobic layers

The polymer chemistry dependency of interactions and dynamics of water in the assemblies was analysed by the survival probability that measures the likelihood of water remaining in the hydrophobic layer for a given time period and the MSD of the water molecules in the hydrophobic layer. The data for the 10% stretched systems is presented in Fig. 7, while Figure S6 of the SI contains the 0% stretched systems data. Reflecting the hydrophobicity differences, in the P(S-BA)-*b*-St and P(S-EHA)-*b*-St assemblies, the time decay of the survival probabilities is faster than in the P(iBM-BA)-*b*-St and P(MMA-BA)-*b*-St assemblies. Aligned with the survival probability response, Fig. 7(b) presents the corresponding MSD data. Consistent with the survival probability decay trends, water mobility is largest in the P(S-BA)-*b*-St and P(S-EHA)-*b*-St systems and P(iBM-BA)-*b*-St and P(MMA-BA)-*b*-St bind water stronger in their hydrophobic layers.

The findings can be directly converted to molecular level understanding for controlling water binding. First, as indicated by Fig. 5, a key to maintaining hydrophobic character in the packing with local stresses and strains present is that the backbones can bend to cover any extra volume created by local strain. Once this is covered, the hydrophobic moieties need to be sufficiently large and flexible to block water even in the stretched state. This is attained by the styrene rings, as shown by the P(S-BA)-*b*-St and P(S-EHA)-*b*-St environments exhibiting fastest water exchange dynamics for any water molecules in the hydrophobic layer and also the largest water mobility. This also directly captures that these environments are less favourable to water molecules in comparison to the slower decay hydrophobic surroundings.

4. Conclusions

In this work, we assessed the ability of four different linear amphiphilic di-block copolymer coatings to block water. This was done via MD simulations to resolve the molecular level dependencies in water interactions with the coatings. The hydrophilic block of all di-block copolymers was starch, whereas the hydrophobic block was varied. In our MD simulations, we found that all examined compositions resulted in films with efficient water-blocking properties due to the relatively ideal, strain-free packing of the polymer chains. However, the key to maintaining the moisture blocking properties under conditions, where the polymer film is strained or the packing is less ideal, is the ability of the hydrophobic block to resiliently adapt to fill voids and form a uniform hydrophobic coating. In this, larger hydrophobic monomers, that have bulky and long chemical side groups, impeded water penetration. We also found that side chain flexibility is important. Overall, our findings are consistent with those of Ref. [115]. Similar outcomes relating the permeability of water molecules with the chemical composition and side chain lengths of polymer components have also been reported in Refs. [23,41,116], yet without extracting direct molecular level information.

In addition to the chemical composition, crystallinity, and the structure of the hydrophobic layers play a crucial role in determining the barrier properties of films and membranes [117–120]. Our findings indicate that a higher level of ordering in the hydrophobic layer indeed correlates with water blocking properties of the assembly. This has been previously associated with a reduction of free volume and segmental mobility [121]. Inversely, water transport through a polymer assembly

is favourable in the presence of percolated free volume [73,122]. Furthermore, we found that stretching of the polymer assemblies decreases the ordering of the hydrophobic layer, leading to enhanced water penetration. The findings of Ref. [123], where applying lateral tension on the polymer assembly led to structural changes and altered the assembly water permeability, are consistent with the structure changes observed here.

We also analysed the hydrophobic/hydrophilic interface changes between the different copolymer systems and the resilience of this interface to stretching. The findings clearly associate the interface smoothness and stability with the efficient blocking of water molecules. This could relate to good barrier performance. Previously, the surface morphology has been reported to directly affect small molecules transport through a polymer assembly [63,67]. Here, we found that a smooth interface enhances molecular level blocking of water. Furthermore, strain may anneal the interface: we observed that two of the four studied systems underwent an increase in the smoothness of the interface when stretched. This led to better performance in terms of blocking water. This is in agreement with the findings of Refs. [33,124], where the level of roughness of the interface has been directly correlated with the probability for water molecules to penetrate through it. For the systems studied here, we note that the polymer assemblies containing styrene monomers annealed their interface roughness upon stretching, and consequently, their water blocking performance improved.

The findings here are important, not only in deciphering the molecular level dependencies of the water blocking response for such copolymers, but also in highlighting the importance of non-idealities in the modelling conditions for correctly capturing the response. Here, we considered lateral stretching as a crude simplification of the effect of general packing irregularity and strain. Importantly, this allows observing which film compositions are resilient to local strain in their water blocking. Overall, the generated molecular level guidelines for film design can bear significance in the design of advanced moisture protection materials.

CRediT authorship contribution statement

Kourosh Hasheminejad: Writing – original draft, Visualization, Methodology, Investigation, Formal analysis, Data curation, Conceptualization. **Ygor Morais Jaques:** Writing – review & editing, Visualization, Methodology. **Anneli Lepo:** Investigation, Conceptualization. **Alberto Scacchi:** Writing – review & editing, Visualization, Conceptualization. **Maria Sammalkorpi:** Writing – review & editing, Supervision, Project administration, Funding acquisition, Conceptualization.

Declaration of competing interest

The authors declare the following financial interests/personal relationships which may be considered as potential competing interests: Anneli Lepo reports a relationship with Kemira Oyj that includes: employment. If there are other authors, they declare that they have no known competing financial interests or personal relationships that could have appeared to influence the work reported in this paper.

Acknowledgements

This work was supported by Business Finland Co-Innovation grant No. 3767/31/2019 (M.S.) and the Academy of Finland, Finland through its Centres of Excellence Programme (2022–2029, LIBER) under project nos. 346111 and 364205 (M.S.) and Academy of Finland, Finland project no. 359180 (M.S). We are grateful for the support by FinnCERES Materials Bioeconomy Ecosystem. Computational resources by CSC IT Centre for Finland and RAMI – RawMatters Finland Infrastructure are gratefully acknowledged. We also acknowledge CSC for awarding this project access to the LUMI supercomputer, owned by the EuroHPC Joint Undertaking, hosted by CSC (Finland) and the LUMI consortium through a CSC project call.

Appendix A. Supplementary data

Supplementary material related to this article can be found online at https://doi.org/10.1016/j.commatsci.2025.114046.

Data availability

Link to the inputs of the simulations and data is provided at https://doi.org/10.23729/fd-b67f2326-a086-3ca5-a757-1436134d5ab6. If using the inputs or the open data, we request acknowledging the authors by a citing the original source (this paper).

References

[1] R. John, K. Pal, J.S. Jayan, S. Appukuttan, K. Joseph, New emerging review on advances in block copolymer based water purification membranes, J. Mol. Struct. 1231 (2021) 129926.
[2] C. Ma, M. Wang, Z. Wang, M. Gao, J. Wang, Recent progress on thin film composite membranes for CO_2 separation, J. CO2 Util. 42 (2020) 101296.
[3] E.R. Radu, S.I. Voicu, V.K. Thakur, Polymeric membranes for biomedical applications, Polymers 15 (3) (2023) 619.
[4] R. John, K. Pal, J.S. Jayan, S. Appukuttan, K. Joseph, New emerging review on advances in block copolymer based water purification membranes, J. Mol. Struct. 1231 (2021) 129926.
[5] L. Guo, Y. Wang, M. Steinhart, Porous block copolymer separation membranes for 21st century sanitation and hygiene, Chem. Soc. Rev. 50 (11) (2021) 6333–6348.
[6] Y. Wu, Y. Ma, Y. Gao, Y. Liu, C. Gao, Poly (lactic acid)-based pH responsive membrane combined with chitosan and alizarin for food packaging, Int. J. Biol. Macromol. 214 (2022) 348–359.
[7] M. Müller, V. Abetz, Nonequilibrium processes in polymer membrane formation: Theory and experiment, Chem. Rev. 121 (22) (2021) 14189–14231.
[8] C. Cummins, R. Lundy, J.J. Walsh, V. Ponsinet, G. Fleury, M.A. Morris, Enabling future nanomanufacturing through block copolymer self-assembly: A review, Nano Today 35 (2020) 100936.
[9] N. Hampu, J.R. Werber, W.Y. Chan, E.C. Feinberg, M.A. Hillmyer, Next-generation ultrafiltration membranes enabled by block polymers, ACS Nano 14 (12) (2020) 16446–16471.
[10] E.A. Jackson, M.A. Hillmyer, Nanoporous membranes derived from block copolymers: From drug delivery to water filtration, ACS Nano 4 (7) (2010) 3548–3553.
[11] A. Mehta, A.L. Zydney, Permeability and selectivity analysis for ultrafiltration membranes, J. Membr. Sci. 249 (1) (2005) 245–249.
[12] F.H. Akhtar, H. Vovushua, L.F. Villalobos, R. Shevate, M. Kumar, S.P. Nunes, U. Schwingenschlögl, K.-V. Peinemann, Highways for water molecules: Interplay between nanostructure and water vapor transport in block copolymer membranes, J. Membr. Sci. 572 (2019) 641–649.
[13] S. Javan Nikkhah, M. Sammalkorpi, Single core and multicore aggregates from a polymer mixture: A dissipative particle dynamics study, J. Colloid Interface Sci. 635 (2023) 231–241.
[14] A.L. Harmat, S. Javan Nikkhah, M. Sammalkorpi, Dissipative particle dynamics simulations of H-shaped diblock copolymer self-assembly in solvent, Polymer 233 (2021) 124198.
[15] Y. Hibi, U. Wiesner, Surface segregation and self-assembly of block-copolymer separation layers on top of homopolymer substructures in asymmetric ultrafiltration membranes from a single casting step, Adv. Funct. Mater. 31 (29) (2021) 2009387.
[16] B.A. Lamers, R. Graf, B.F. de Waal, G. Vantomme, A.R. Palmans, E. Meijer, Polymorphism in the assembly of phase-segregated block molecules: Pathway control to 1D and 2D nanostructures, J. Am. Chem. Soc. 141 (38) (2019) 15456–15463.
[17] B.M. Trinh, B.P. Chang, T.H. Mekonnen, The barrier properties of sustainable multiphase and multicomponent packaging materials: A review, Prog. Mater. Sci. 133 (2023) 101071.
[18] C. Zhang, C. Ma, X. Yao, X. Yang, W. Zhang, G. Zhang, Transparent and flexible vesicles/lamellae mixed matrix organic-bridged polysilsesquioxane coatings as water vapor barrier, Prog. Org. Coat. 174 (2023) 107236.
[19] J. Wang, J.P. DeRocher, L. Wu, F.S. Bates, E. Cussler, Barrier films made with various lamellar block copolymers, J. Membr. Sci. 270 (1) (2006) 13–21.
[20] V. Roche, F. Vacandio, D. Bertin, D. Gigmes, M. Eyraud, Block copolymers for corrosion protection of aluminium, C. R. Chim. 11 (9) (2008) 1055–1062.
[21] S.C. George, S. Thomas, Transport phenomena through polymeric systems, Prog. Polym. Sci. 26 (6) (2001) 985–1017.
[22] J. Lagaron, R. Catalá, R. Gavara, Structural characteristics defining high barrier properties in polymeric materials, Mater. Sci. Technol. 20 (1) (2004) 1–7.

[23] D.J. Woods, S.A. Hillman, D. Pearce, L. Wilbraham, L.Q. Flagg, W. Duffy, I. McCulloch, J.R. Durrant, A.A. Guilbert, M.A. Zwijnenburg, R.S. Sprick, J. Nelson, A.I. Cooper, Side-chain tuning in conjugated polymer photocatalysts for improved hydrogen production from water, Energy Environ. Sci. 13 (6) (2020) 1843–1855.
[24] Z. Yu, Y. Ji, V. Bourg, M. Bilgen, J.C. Meredith, Chitin-and cellulose-based sustainable barrier materials: A review, Emergent Mater. 3 (2020) 919–936.
[25] H. Zhu, Z. Guo, W. Liu, Adhesion behaviors on superhydrophobic surfaces, Chem. Commun. 50 (30) (2014) 3900–3913.
[26] R.R. Netz, D. Andelman, Roughness-induced wetting, Phys. Rev. E 55 (1) (1997) 687.
[27] B. Samuel, H. Zhao, K.-Y. Law, Study of wetting and adhesion interactions between water and various polymer and superhydrophobic surfaces, J. Phys. Chem. C 115 (30) (2011) 14852–14861.
[28] E. Yilgör, C.K. Söz, I. Yilgör, Wetting behavior of superhydrophobic poly (methyl methacrylate), Prog. Org. Coat. 125 (2018) 530–536.
[29] K. Grundke, K. Pöschel, A. Synytska, R. Frenzel, A. Drechsler, M. Nitschke, A. Cordeiro, P. Uhlmann, P. Welzel, Experimental studies of contact angle hysteresis phenomena on polymer surfaces — Toward the understanding and control of wettability for different applications, Adv. Colloid Interface Sci. 222 (2015) 350–376.
[30] Y. Wang, G. Meresi, J. Gosselin, D. Azar, Wen, A.A. Jones, P.T. Inglefield, Diffusion of decafluoropentane in amorphous glassy perfluorodioxole copolymer by pulse field gradient NMR spectroscopy, Macromolecules 34 (19) (2001) 6680–6683.
[31] D.T. Hallinan, Y.A. Elabd, Diffusion and sorption of methanol and water in nafion using time-resolved Fourier transform infrared-attenuated total reflectance spectroscopy, J. Phys. Chem. B 111 (46) (2007) 13221–13230.
[32] S.B. Black, Y. Chang, C. Bae, M.A. Hickner, FTIR characterization of water–polymer interactions in superacid polymers, J. Phys. Chem. B 117 (50) (2013) 16266–16274.
[33] Z.A. Boeva, A. Catena, L. Höfler, S. Wehner, C.B. Fischer, T. Lindfors, Improved water barrier properties of polylactic acid films with an amorphous hydrogenated carbon (a-C:H) coating, Carbon 120 (2017) 157–164.
[34] J. Pavelec, D. DiGuiseppi, B.Y. Zavlavsky, V.N. Uversky, R. Schweitzer-Stenner, Perturbation of water structure by water-polymer interactions probed by FTIR and polarized Raman spectroscopy, J. Mol. Liq. 275 (2019) 463–473.
[35] L. He, H.L. Smith, J. Majewski, C.H. Fujimoto, C.J. Cornelius, D. Perahia, Interfacial effects on water penetration into ultrathin ionomer films: An in situ study using neutron reflectometry, Macromolecules 42 (15) (2009) 5745–5751.
[36] E.P. Chan, B.R. Frieberg, K. Ito, J. Tarver, M. Tyagi, W. Zhang, E.B. Coughlin, C.M. Stafford, A. Roy, S. Rosenberg, C.L. Soles, Insights into the water transport mechanism in polymeric membranes from neutron scattering, Macromolecules 53 (4) (2020) 1443–1450.
[37] J. Li, M. Pan, H. Tang, Understanding short-side-chain perfluorinated sulfonic acid and its application for high temperature polymer electrolyte membrane fuel cells, RSC Adv. 4 (8) (2014) 3944–3965.
[38] L. Jin, J. Tian, J. Li, X. Yan, D. Qi, Investigation of the water barrier properties of graft copolymer latex films of acrylate and poly(dimethylsiloxane) macromonomers synthesized by RAFT miniemulsion polymerization, Eur. Polym. J. 168 (2022) 111107.
[39] I. Yilgor, S. Bilgin, M. Isik, E. Yilgor, Tunable wetting of polymer surfaces, Langmuir 28 (41) (2012) 14808–14814.
[40] E. Caliskan, S. Shishatskiy, S. Neumann, V. Abetz, V. Filiz, Investigation of the side chain effect on gas and water vapor transport properties of anthracene-maleimide based polymers of intrinsic microporosity, Polymers 14 (1) (2021) 119.
[41] J. Liao, X. Yu, Q. Chen, X. Gao, H. Ruan, J. Shen, C. Gao, Monovalent anion selective anion-exchange membranes with imidazolium salt-terminated side-chains: Investigating the effect of hydrophobic alkyl spacer length, J. Membr. Sci. 599 (2020) 117818.
[42] S. Morsch, S. Lyon, P. Greensmith, S. Smith, S. Gibbon, Mapping water uptake in organic coatings using AFM-IR, Faraday Discuss. 180 (2015) 527–542.
[43] N.B. McKeown, P.M. Budd, Exploitation of intrinsic microporosity in polymer-based materials, Macromolecules 43 (12) (2010) 5163–5176.
[44] S. Luo, J. Leisen, C. Wong, Study on mobility of water and polymer chain in epoxy and its influence on adhesion, J. Appl. Polym. Sci. 85 (1) (2002) 1–8.
[45] L.Q. Flagg, C.G. Bischak, J.W. Onorato, R.B. Rashid, C.K. Luscombe, D.S. Ginger, Polymer crystallinity controls water uptake in glycol side-chain polymer organic electrochemical transistors, J. Am. Chem. Soc. 141 (10) (2019) 4345–4354.
[46] A. Phan, D. Fan, A. Striolo, Fluid transport through heterogeneous pore matrices: Multiscale simulation approaches, Phys. Fluids 32 (10) (2020).
[47] A.-M. Schmidt, Y. Kyosev, Particle based simulation of the polymer penetration into porous structures during the fused deposition modelling, J. Manuf. Process. 101 (2023) 1205–1213.
[48] C. Huang, Y. Zhu, X. Man, Block copolymer thin films, Phys. Rep. 932 (2021) 1–36.
[49] M. Müller, Process-directed self-assembly of copolymers: Results of and challenges for simulation studies, Prog. Polym. Sci. 101 (2020) 101198.
[50] K. Hasheminejad, A. Scacchi, S. Javan Nikkhah, M. Sammalkorpi, Cracking polymer coatings of paper-like surfaces: Control via block co-polymer structure and system composition, Appl. Surf. Sci. 640 (2023) 158324.
[51] A. Scacchi, K. Hasheminejad, S. Javan Nikkhah, M. Sammalkorpi, Controlling self-assembling co-polymer coatings of hydrophilic polysaccharide substrates via co-polymer block length ratio, J. Colloid Interface Sci. 640 (2023) 809–819.
[52] A.P. Lindsay, G.K. Cheong, A.J. Peterson, S. Weigand, K.D. Dorfman, T.P. Lodge, F.S. Bates, Complex phase behavior in particle-forming AB/AB' diblock copolymer blends with variable core block lengths, Macromolecules 54 (15) (2021) 7088–7101.
[53] M.W. Matsen, Effect of architecture on the phase behavior of AB-type block copolymer melts, Macromolecules 45 (4) (2012) 2161–2165.
[54] P. Batys, S. Kivistö, S.M. Lalwani, J.L. Lutkenhaus, M. Sammalkorpi, Comparing water-mediated hydrogen-bonding in different polyelectrolyte complexes, Soft Matter 15 (2019) 7823–7831.
[55] Y. Zhang, P. Batys, J.T. O'Neal, F. Li, M. Sammalkorpi, J.L. Lutkenhaus, Molecular origin of the glass transition in polyelectrolyte assemblies, ACS Cent. Sci. 4 (5) (2018) 638–644.
[56] S. Zid, M. Zinet, E. Espuche, Modeling diffusion mass transport in multiphase polymer systems for gas barrier applications: A review, J. Polym. Sci. Part B: Polym. Phys. 56 (8) (2018) 621–639.
[57] X. Fang, O. Vitrac, Predicting diffusion coefficients of chemicals in and through packaging materials, Crit. Rev. Food Sci. Nutr. 57 (2) (2017) 275–312.
[58] N. Zhang, S. Chen, B. Yang, J. Huo, X. Zhang, J. Bao, X. Ruan, G. He, Effect of hydrogen-bonding interaction on the arrangement and dynamics of water confined in a polyamide membrane: A molecular dynamics simulation, J. Phys. Chem. B 122 (17) (2018) 4719–4728.
[59] J. Liu, J. Jiang, Molecular design of microporous polymer membranes for the upgrading of natural gas, J. Phys. Chem. C 123 (11) (2019) 6607–6615.
[60] M. Kanduč, W.K. Kim, R. Roa, J. Dzubiella, Aqueous nanoclusters govern ion partitioning in dense polymer membranes, ACS Nano 13 (10) (2019) 11224–11234.
[61] M. Kanduč, W.K. Kim, R. Roa, J. Dzubiella, How the shape and chemistry of molecular penetrants control responsive hydrogel permeability, ACS Nano 15 (1) (2020) 614–624.
[62] R. Kali, S.T. Milner, Simulations predict salt partitioning in nanostructured ion exchange membranes, J. Membr. Sci. 697 (2024) 122582.
[63] J. Muscatello, E. Müller, A. Mostofi, A. Sutton, Multiscale molecular simulations of the formation and structure of polyamide membranes created by interfacial polymerization, J. Membr. Sci. 527 (2017) 180–190.
[64] A. Gautieri, S. Vesentini, A. Redaelli, How to predict diffusion of medium-sized molecules in polymer matrices. from atomistic to coarse grain simulations, J. Mol. Model. 16 (2010) 1845–1851.
[65] S. Nawaz, P. Carbone, Coarse-graining poly (ethylene oxide)–poly (propylene oxide)–poly (ethylene oxide)(PEO–PPO–PEO) block copolymers using the MARTINI force field, J. Phys. Chem. B 118 (6) (2014) 1648–1659.
[66] C.F. Lopez, S.O. Nielsen, G. Srinivas, W.F. DeGrado, M.L. Klein, Probing membrane insertion activity of antimicrobial polymers via coarse-grain molecular dynamics, J. Chem. Theory Comput. 2 (3) (2006) 649–655.
[67] Y. Araki, Y. Kobayashi, T. Kawaguchi, T. Kaneko, N. Arai, Water permeation in polymeric membranes: Mechanism and synthetic strategy for water-inhibiting functional polymers, J. Membr. Sci. 564 (2018) 184–192.
[68] R.M. Venable, A. Kramer, R.W. Pastor, Molecular dynamics simulations of membrane permeability, Chem. Rev. 119 (9) (2019) 5954–5997.
[69] S. Moradi, A. Nowroozi, M. Shahlaei, Shedding light on the structural properties of lipid bilayers using molecular dynamics simulation: A review study, RSC Adv. 9 (8) (2019) 4644–4658.
[70] A. Krämer, A. Ghysels, E. Wang, R.M. Venable, J.B. Klauda, B.R. Brooks, R.W. Pastor, Membrane permeability of small molecules from unbiased molecular dynamics simulations, J. Chem. Phys. 153 (12) (2020).
[71] W. Shinoda, Permeability across lipid membranes, Biochim. Biophys. Acta (BBA)- Biomembr. 1858 (10) (2016) 2254–2265.
[72] E. Awoonor-Williams, C.N. Rowley, Molecular simulation of nonfacilitated membrane permeation, Biochim. Biophys. Acta 1858 (7) (2016) 1672–1687.
[73] M. Shen, S. Keten, R.M. Lueptow, Dynamics of water and solute transport in polymeric reverse osmosis membranes via molecular dynamics simulations, J. Membr. Sci. 506 (2016) 95–108.
[74] J. Shen, Y. Cai, C. Zhang, W. Wei, C. Chen, L. Liu, K. Yang, Y. Ma, Y. Wang, C.-C. Tseng, J.-H. Fu, X. Dong, J. Li, X.-X. Zhang, L.-J. Li, J. Jiang, I. Pinnau, V. Tung, Y. Han, Fast water transport and molecular sieving through ultrathin ordered conjugated-polymer-framework membranes, Nat. Mater. 21 (10) (2022) 1183–1190.
[75] R. Cui, S. Li, C. Yu, Y. Wang, Y. Zhou, Understanding the mechanism of nitrogen transport in the perfluorinated sulfonic-acid hydrated membranes via molecular dynamics simulations, J. Membr. Sci. 648 (2022) 120328.
[76] M.V. Ramos-Garcés, D.I. Senadheera, K. Arunagiri, P.P. Angelopoulou, G. Sakellariou, K. Li, B.D. Vogt, R. Kumar, C.G. Arges, Ion transport on self-assembled block copolymer electrolytes with different side chain chemistries, Mater. Adv. 4 (3) (2023) 965–975.

[77] Z. Zhang, Y. Han, W.-R. Chen, C. Do, Diffusion characteristics of water molecules in a lamellar structure formed by triblock copolymers, Phys. Chem. Chem. Phys. 24 (13) (2022) 8015–8021.
[78] M. Senanayake, D. Aryal, G.S. Grest, D. Perahia, Interfacial response and structural adaptation of structured polyelectrolyte thin films, Macromolecules 54 (6) (2021) 2892–2898.
[79] C.I. Eneh, T. Kastinen, S. Oka, P. Batys, M. Sammalkorpi, J.L. Lutkenhaus, Quantification of water–ion pair interactions in polyelectrolyte multilayers using a quartz crystal microbalance method, ACS Polym. Au 2 (4) (2022) 287–298.
[80] J. Wang, J.P. DeRocher, L. Wu, F.S. Bates, E. Cussler, Barrier films made with various lamellar block copolymers, J. Membr. Sci. 270 (1–2) (2006) 13–21.
[81] J.N. Albert, T.H. Epps III, Self-assembly of block copolymer thin films, Mater. Today 13 (6) (2010) 24–33.
[82] R. Kali, E. Andini, S.T. Milner, Molecular dynamics simulation based design of biomimetic membrane with artificial water channels, J. Membr. Sci. 630 (2021) 119279.
[83] G. Srinivas, J.C. Shelley, S.O. Nielsen, D.E. Discher, M.L. Klein, Simulation of diblock copolymer self-assembly, using a coarse-grain model, J. Phys. Chem. B 108 (24) (2004) 8153–8160.
[84] O.L. Torres-Rocha, S. Campbell, N. Woodcock, J. Pinaud, P. Lacroix-Desmazes, P. Champagne, M.F. Cunningham, Non-covalent polymer surface modification of cellulose nanocrystals using block copolymers, Macromol. React. Eng. 16 (3) (2022) 2100046.
[85] P. Tyagi, K.S. Salem, M.A. Hubbe, L. Pal, Advances in barrier coatings and film technologies for achieving sustainable packaging of food products - a review, Trends Food Sci. Technol. 115 (2021) 461–485.
[86] H. Li, Y. Qi, Y. Zhao, J. Chi, S. Cheng, Starch and its derivatives for paper coatings: A review, Prog. Org. Coat. 135 (2019) 213–227.
[87] S. Cheng, Y. Zhang, Y. Wu, Preparation and characterization of enzymatically degraded starch-g-poly (styrene-co-butyl acrylate) latex for paper coating, Polym.-Plast. Technol. Eng. 53 (17) (2014) 1811–1816.
[88] N. Nemati, F.A. Taromi, M. Mirzataheri, In-situ water based emulsion copolymerization of styrene/ethylhexyl acrylate in presence of cloisite 15A, Procedia Mater. Sci. 11 (2015) 542–547.
[89] F.M. Silva, R.J. Pinto, A. Barros-Timmons, C.S. Freire, Solventless photopolymerizable paper coating formulation for packaging applications, Polymers 15 (5) (2023) 1069.
[90] A. Chaiyasat, H. Kobayashi, M. Okubo, Incorporation of nonionic emulsifier inside methacrylic polymer particles in emulsion polymerization, Colloid Polym. Sci. 285 (2007) 557–562.
[91] K. Kaneko, M. Hara, T. Nishino, T. Maruyama, One-step biotinylation of cellulose paper by polymer coating to prepare a paper-based analytical device, Anal. Chem. 92 (2) (2019) 1978–1987.
[92] Y. Liu, J. Hu, Investigation of polystyrene-based microspheres from different copolymers and their structural color coatings on wood surface, Coatings 11 (1) (2020) 14.
[93] L.D. Rodrigues, C.R. Hurtado, E.F. Macedo, D.B. Tada, L.M. Guerrini, M.P. Oliveira, Colloidal properties and cytotoxicity of enzymatically hydrolyzed cationic starch-graft-poly (butyl acrylate-co-methyl methacrylate) latex by surfactant-free emulsion polymerization for paper coating application, Prog. Org. Coat. 145 (2020) 105693.
[94] A.P. Thompson, H.M. Aktulga, R. Berger, D.S. Bolintineanu, W.M. Brown, P.S. Crozier, P.J. in 't Veld, A. Kohlmeyer, S.G. Moore, T.D. Nguyen, R. Shan, M.J. Stevens, J. Tranchida, C. Trott, S.J. Plimpton, LAMMPS - a flexible simulation tool for particle-based materials modeling at the atomic, meso, and continuum scales, Comput. Phys. Comm. 271 (2022) 108171.
[95] W.L. Jorgensen, D.S. Maxwell, J. Tirado-Rives, Development and testing of the OPLS all-atom force field on conformational energetics and properties of organic liquids, J. Am. Chem. Soc. 118 (45) (1996) 11225–11236.
[96] W. Damm, A. Frontera, J. Tirado-Rives, W.L. Jorgensen, OPLS all-atom force field for carbohydrates, J. Comput. Chem. 18 (16) (1997) 1955–1970.
[97] M.L. Price, D. Ostrovsky, W.L. Jorgensen, Gas-phase and liquid-state properties of esters, nitriles, and nitro compounds with the OPLS-AA force field, J. Comput. Chem. 22 (13) (2001) 1340–1352.
[98] D.J. Price, C.L. Brooks III, A modified TIP3P water potential for simulation with Ewald summation, J. Chem. Phys. 121 (20) (2004) 10096–10103.
[99] E.S. Cho, C.M. Evans, E.C. Davidson, M.L. Hoarfrost, M.A. Modestino, R.A. Segalman, J.J. Urban, Enhanced water vapor blocking in transparent hybrid polymer–nanocrystal films, ACS Macro Lett. 4 (1) (2015) 70–74.
[100] M.D. Hanwell, D.E. Curtis, D.C. Lonie, T. Vandermeersch, E. Zurek, G.R. Hutchison, Avogadro: An advanced semantic chemical editor, visualization, and analysis platform, J. Cheminform. 4 (1) (2012) 1–17.
[101] A.I. Jewett, D. Stelter, J. Lambert, S.M. Saladi, O.M. Roscioni, M. Ricci, L. Autin, M. Maritan, S.M. Bashusqeh, T. Keyes, R.T. Dame, J.-E. Shea, G.J. Jensen, D.S. Goodsell, Moltemplate: A tool for coarse-grained modeling of complex biological matter and soft condensed matter physics, J. Mol. Biol. 433 (11) (2021) 166841.
[102] L. Martínez, R. Andrade, E.G. Birgin, J.M. Martínez, PACKMOL: A package for building initial configurations for molecular dynamics simulations, J. Comput. Chem. 30 (13) (2009) 2157–2164.
[103] A. Stukowski, Visualization and analysis of atomistic simulation data with OVITO-the open visualization tool, Modelling Simul. Mater. Sci. Eng. 18 (1) (2009) 015012.
[104] R.J. Gowers, M. Linke, J. Barnoud, T.J. Reddy, M.N. Melo, S.L. Seyler, J. Domanski, D.L. Dotson, S. Buchoux, I.M. Kenney, O. Beckstein, MDAnalysis: a python package for the rapid analysis of molecular dynamics simulations, in: S. Benthall, S. Rostrup (Eds.), Proceedings of the 15th Python in Science Conference, SciPy, Austin, TX, 2016.
[105] N. Michaud-Agrawal, E.J. Denning, T.B. Woolf, O. Beckstein, MDAnalysis: a toolkit for the analysis of molecular dynamics simulations, J. Comput. Chem. 32 (10) (2011) 2319–2327.
[106] S. Nosé, A unified formulation of the constant temperature molecular dynamics methods, J. Chem. Phys. 81 (1) (1984) 511–519.
[107] W.G. Hoover, Canonical dynamics: Equilibrium phase-space distributions, Phys. Rev. A 31 (3) (1985) 1695.
[108] W.G. Hoover, Constant-pressure equations of motion, Phys. Rev. A 34 (3) (1986) 2499.
[109] R.N. Wenzel, Resistance of solid surfaces to wetting by water, Ind. Eng. Chem. 28 (8) (1936) 988–994.
[110] A. Stukowski, Computational analysis methods in atomistic modeling of crystals, J. Miner. Met. Mater. Soc. 66 (2014) 399–407.
[111] L.B. Pártay, G. Hantal, P. Jedlovszky, Á. Vincze, G. Horvai, A new method for determining the interfacial molecules and characterizing the surface roughness in computer simulations. Application to the liquid–vapor interface of water, J. Comput. Chem. 29 (6) (2008) 945–956.
[112] M.P. Allen, D.J. Tildesley, Computer Simulation of Liquids, second ed., Oxford University Press, Oxford, UK, 2017.
[113] K. He, F. Babaye Khorasani, S.T. Retterer, D.K. Thomas, J.C. Conrad, R. Krishnamoorti, Diffusive dynamics of nanoparticles in arrays of nanoposts, ACS Nano 7 (6) (2013) 5122–5130.
[114] P. Liu, E. Harder, B. Berne, On the calculation of diffusion coefficients in confined fluids and interfaces with an application to the liquid-vapor interface of water, J. Phys. Chem. B 108 (21) (2004) 6595–6602.
[115] A.-T. Kuo, S. Urata, R. Koguchi, T. Sonoda, S. Kobayashi, M. Tanaka, Molecular dynamics study on the water mobility and side-chain flexibility of hydrated poly (ω-methoxyalkyl acrylate)s, ACS Biomater. Sci. Eng. 6 (12) (2020) 6690–6700.
[116] E. Caliskan, S. Shishatskiy, S. Neumann, V. Abetz, V. Filiz, Investigation of the side chain effect on gas and water vapor transport properties of anthracene-maleimide based polymers of intrinsic microporosity, Polymers 14 (1) (2022) 119.
[117] T.-W. Lin, B. Mei, K.S. Schweizer, C.E. Sing, Simulation study of the effects of polymer network dynamics and mesh confinement on the diffusion and structural relaxation of penetrants, J. Chem. Phys. 159 (2023) 014904.
[118] D. Aryal, A. Agrawal, D. Perahia, G.S. Grest, Structured ionomer thin films at water interface: Molecular dynamics simulation insight, Langmuir 33 (41) (2017) 11070–11076.
[119] L. Jin, J. Tian, J. Li, X. Yan, D. Qi, Investigation of the water barrier properties of graft copolymer latex films of acrylate and poly (dimethylsiloxane) macromonomers synthesized by RAFT miniemulsion polymerization, Eur. Polym. J. 168 (2022) 111107.
[120] Y. Prykhodko, A. Martin, H. Oulyadi, S. Marais, K. Fatyeyeva, Polymer EVA-OH membrane with improved water/gas separation performance: Influence of VAc/VOH repeating units ratio on membrane physical chemical properties, J. Membr. Sci. 673 (2023) 121386.
[121] K. Prasad, M. Nikzad, I. Sbarski, Permeability control in polymeric systems: A review, J. Polym. Res. 25 (2018) 1–20.
[122] Y. Wang, Q. Wei, S. Wang, W. Chai, Y. Zhang, Structural and water diffusion of poly (acryl amide)/poly (vinyl alcohol) blend films: Experiment and molecular dynamics simulations, J. Mol. Graph. Model. 71 (2017) 40–49.
[123] A.S. Reddy, D.T. Warshaviak, M. Chachisvilis, Effect of membrane tension on the physical properties of DOPC lipid bilayer membrane, Biochim. Biophys. Acta 1818 (9) (2012) 2271–2281.
[124] C.-D. Wu, L.-M. Kuo, S.-J. Lin, T.-H. Fang, S.-F. Hsieh, Effects of temperature, size of water droplets, and surface roughness on nanowetting properties investigated using molecular dynamics simulation, Comput. Mater. Sci. 53 (1) (2012) 25–30.